Nonlinear atomic spectroscopy inside a random porous medium

S. Villalba, H. Failache, L. Lenci, and A. Lezama*

Instituto de Física, Facultad de Ingeniería, Universidad de la República, J. Herrera y Reissig 565, 11300 Montevideo, Uruguay

(Received 20 October 2014; published 20 November 2014)

We have studied the pump-probe spectroscopy of rubidium vapor confined to the micrometric interstices of a random porous glass. Due to the propagation in the highly scattering medium, the light fields are randomized inside the sample with significant consequences for the atomic spectra. A two-frequency modulation technique was used to isolate the atomic response proportional to the product of the intensities of the pump and probe fields. Unusual line shapes were observed which include relatively narrow structures that are present in spite of the Doppler broadening due to the atomic velocity distribution. A simple theoretical modeling of the light-atom interaction that assumes statistical isotropy of the diffuse light field and mutual temporal incoherence of the pump and probe fields is presented. Using a single adjustable parameter to account for the atomic confinement, the model successfully describes the diversity of the observed spectral line shapes.

DOI: 10.1103/PhysRevA.90.052518 PACS number(s): 32.30.−r, 42.62.Fi, 42.25.Dd, 32.70.Jz

I. INTRODUCTION

The spectra of atoms confined to small volumes present interesting differences with those of atomic vapors observed in standard spectroscopic cells. In thin cells, where the atoms are confined within two parallel windows separated by several microns, sub-Doppler spectral features appear in the linear interaction of the atoms with laser light [1,2]. Nanometric thin cells, with a window separation comparable to the optical wavelength, have been used to observe the enhancement of the coherent transient atomic response due to Dicke narrowing and to study long-range atom-wall interactions [3,4]. Nanocells have been also used to study either new physical phenomena such as the cooperative Lamb shift [5] or the enhanced optical response of high density Rb vapor [6]. More recently, electromagnetically induced transparency (EIT) resonances have been observed in micrometric thin cells [7–9] and even in nanometric thin cells [10,11].

In parallel to the interest for the spectroscopy of atoms under confinement, the use of diffuse light for spectroscopy purposes has attracted increased attention in the last few years. Light diffusion in strongly scattering media allows long effective light paths that can be used for sensitive spectroscopy in a reduced volume [12–14] and for the construction of miniaturized spectrometers [15]. Sub-Doppler spectroscopic signals were observed in a linear regime in the backscattered light from a photonic crystal of nanospheres infused with Cs [16]. Diffuse light is also at the core of the research on random lasers [17,18] and weak and strong Anderson localization (see Ref. [19], and references therein).

In a recent work [20], we have reported a study of the resonance spectroscopy of Rb inside a random porous glass medium. In such a medium, the atomic motion is limited by the pore dimensions, resulting in reduced light-atom interaction times due to collisions with the pore walls. We have shown that, as a consequence of the spatial randomization of the light wave vector due to diffusive propagation in the porous medium, the laser photons cannot be distinguished from those spontaneously emitted by the atoms. A striking consequence is that almost no absorption is observed on the light scattered through the medium since the photons absorbed by the atoms are almost entirely compensated by fluorescence. For higher atomic densities, such compensation is less effective as photon trapping increases the probability for an excited atom to collide with the pore surface and decay nonradiatively. The same porous medium shows sub-Doppler resonances in the backscattered light due to saturated absorption of the Rb vapor in the interstices of the medium near its surface [21].

In this paper we study the nonlinear response to two laser fields—a pump and a probe—of Rb atoms confined to the micrometric interstices of porous glass. Both laser fields are independently and strongly scattered by the porous medium, giving rise to stochastic spatial variations of their phase, amplitude, and polarization over short distances (typically of the order of the wavelength). The interaction of such *random* light with atoms possessing *random* velocities inside *random* pore volumes gives rise to several interesting problems. Harnessing this triple randomness might appear to be a considerable challenge. In fact, as will be shown below, considerable simplification results when the observed quantities are statistical averages over the ensemble.

Two mechanisms can be pinpointed as the origin of a nonlinear atomic response proportional to the product of the powers of the two fields. One mechanism is saturation: The presence of one field resonant with an atomic transition reduces the population difference between the ground and the excited level, rendering the transition more transparent to the second field. A second mechanism is optical pumping, where atoms excited from one ground level decay by spontaneous emission into a different ground level.

II. EXPERIMENTAL SETUP

The porous sample cells were built following the procedure described in Refs. [20,21]. The porous medium is obtained from ground glass followed by sinterization. The glass grains that compose the porous material are roughly selected by the use of a passing and a retaining mesh. Two different porous glass cells filled with rubidium vapor were used in the experiment. The first cell was made with glass grains that had passed through a 200-μm mesh and were retained by a 74-μm mesh.

*alezama@fing.edu.uy

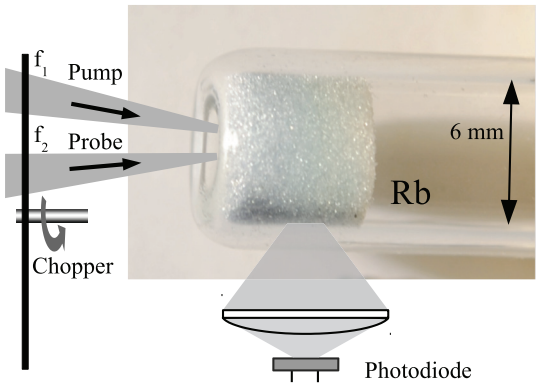

FIG. 1. (Color online) Scheme of the experimental setup showing the porous cell (picture) and detection optics. The collecting lens produces the image of a portion of the porous glass surface on the photodetector. The cell is placed inside an oven (not shown). A chopper wheel modulates the pump- and probe-laser beams at frequencies f_1 and f_2. The $f_1 + f_2$ frequency component of the photodetector output is extracted with a lock-in amplifier (not shown).

We will call this the large-grain cell. The second cell, designated as the small-grain cell, was made with ground glass having passed through a 54-μm mesh. A sedimentation column is used for additional grain size selectivity. The typical size of the interstitial pores ranges between 10 and 100 μm, depending on the sample. The porous material is placed at the flat end of a cylindrical 6-mm-diam glass tube. After inserting a drop of metallic rubidium, the tube is sealed under vacuum. During the experiments, the cell was heated to 120 °C inside an oven with optical windows to increase the atomic vapor density.

The scheme of the experimental setup is presented in Fig. 1. We use two different extended cavity diode lasers operating around the D_1 transitions of Rb (795 nm). The pump laser, when working at resonance or at a crossover frequency, was frequency stabilized on a saturated absorption setup. A stabilization system was not used when working at other frequencies, as the laser was stable enough to be kept at a constant frequency without the use of an active control. The probe laser is tunable and a second saturation absorption setup is used as a frequency reference. The two laser beams are weakly focused on different spots of the nearly flat end of the sample cylinder. The powers of the pump and probe lasers are typically 15 and 10 mW, respectively. A significant reduction of the light intensity inside the porous volume is expected as a consequence of the diffusive propagation in the sample. A small fraction of the light emerging from the cylindrical surface of the sample is collected by a lens and directed into a photodiode.

In order to be sensitive only to the nonlinear atomic response proportional to the two laser field intensities, we have implemented a double-modulation signal detection. The two laser beams were modulated at different frequencies using a chopper. We use a lock-in amplifier to extract the signal modulated at the sum of the two chopping frequencies.

III. MODEL

In order to calculate the nonlinear atomic response we first evaluate, as a function of the pump and probe frequencies, the number of atoms simultaneously resonant with the two fields, taking into account the distribution of atomic velocities in the vapor and the Doppler effect. For this calculation we neglect the homogeneous width of the transition, which is assumed to be much smaller than the typical Doppler width. Once the number of double-resonant atoms for a given pair of atomic transitions is known, we estimate its contribution to the signal.

The main mechanisms responsible for light power variations at the detector are energy loss by nonradiative decay of excited atoms colliding with the pore walls and resonant scattering of the light into propagation modes not directed to the detector. Based on our previous study [20], we believe the first mechanism to be dominant. In any case, the two mechanisms are proportional to the excited-state population. In consequence, we use the calculated excited-state atomic population as a measure of the variation of the photodetector output.

The excited-state population is calculated for a given energy-level configuration using rate equations. The use of rate equations in this context is naturally justified by the assumption that coherence effects are statistically averaged. The signal processing technique used in our experiment allows one to extract from the detector output the contribution proportional to the product of the two field intensities. To estimate such a signal, we expand the exact expression of the excited-state population obtained from the solution of the rate equations into a power series of the field intensities and retain only the lowest-order term proportional to the product of the intensities.

A. Calculation of the number of double-resonant atoms

The basic assumption of our model is that the two laser fields (pump and probe) are completely and independently randomized by scattering in the porous medium. In consequence, at any position in the sample the fields can be considered as a statistically isotropic random superposition of plane waves, each characterized by its wave vector. We calculate the number of atoms interacting with the two fields by determining the atoms simultaneously resonant with a given pair of pump and probe plane waves and assuming that the contributions of all possible pairs can be incoherently added.

Let the frequency of the pump field be $\omega_0 + \Delta$ and that of the probe field $\omega_1 + \delta$, where ω_0 and ω_1 are two atomic transition frequencies ($\delta, \Delta \ll \omega_0, \omega_1$). We initially assume that the pump field wave vector is directed along z while the probe field wave vector lies in the xz plane, forming an angle θ with the z axis. Let $\vec{v} = (v_x, v_y, v_z)$ be the atomic velocity.

The Maxwell velocity distribution for the x and z velocity components is

$$N(v_x, v_z) = \frac{N_0}{2\pi\sigma^2} e^{-\frac{(v_x^2+v_z^2)}{2\sigma^2}}, \tag{1}$$

where N_0 is the total number of atoms in the sample and $\sigma^2 = \frac{k_B T}{m}$ (k_B is the Boltzmann constant, T is temperature, and m is the atom mass).

Neglecting the atomic transition homogeneous width, the resonance conditions for the two fields are

$$k_0 v_z = \Delta, \tag{2}$$

$$k_1 v_x \sin\theta = \delta - \Delta\cos\theta, \tag{3}$$

with $k_i = \omega_i/c$. In consequence, the number of double-resonant atoms is

$$N(\delta,\Delta) = \frac{N_0}{\pi D^2} e^{-\frac{\Delta^2 \sin^2\theta + (\delta - \Delta\cos\theta)^2}{D^2 \sin^2\theta}}, \tag{4}$$

where we have introduced the e^{-1} Doppler half width $D \equiv \sqrt{2}k\sigma$ and neglected a small difference between k_0 and k_1 ($k = k_0 \simeq k_1$). Equation (4) shows that $N(\delta,\Delta)$ is a Gaussian function of δ centered at $\delta = \Delta\cos\theta$ with an e^{-1} width $D\sin\theta$.

We now generalize the previous expression by considering that the probe field wave vector is oriented along the direction defined by the polar angles θ and φ. Assuming a uniform distribution of the probe waves over a solid angle and integrating over all possible orientations of the probe,

$$N(\delta,\Delta) = \frac{N_0}{2\pi D^2} \int_0^{\pi} e^{-\frac{\Delta^2 \sin^2\theta + (\delta - \Delta\cos\theta)^2}{D^2 \sin^2\theta}} \sin\theta d\theta. \tag{5}$$

Finally, introducing the variable change $\cos\theta = u$, we get

$$N(\delta,\Delta) = \frac{N_0}{2\pi D^2} \int_{-1}^{+1} e^{-\frac{(\Delta^2+\delta^2-2u\delta\Delta)}{D^2(1-u^2)}} du. \tag{6}$$

This expression corresponds to a sum of Gaussian functions of δ with width $D\sqrt{1-u^2}$ and whose centers are spread over the interval $[-\Delta, +\Delta]$.

Equation (6) was obtained under the assumption that the pump field has a well-defined orientation. However, the isotropy of the light propagation inside the sample ensures that it remains valid even when the pump field is composed of an incoherent sum of randomly oriented waves. Assuming that the pump field has a fixed detuning Δ and that its spectral width is ε ($\varepsilon \ll D$), we get the distribution $\mathcal{N}(\delta)$ of double-resonant atoms as a function of the probe detuning δ:

$$\mathcal{N}(\delta) = \frac{N_0\varepsilon}{2\pi D^2} \int_{-1}^{+1} e^{-\frac{(\Delta^2+\delta^2-2u\delta\Delta)}{D^2(1-u^2)}} du. \tag{7}$$

Figure 2 shows the distribution function $\mathcal{N}(\delta)$ calculated for a single transition atom ($\omega_1 = \omega_0$) for two different values of the pump detuning Δ. For comparison, a Gaussian with an e^{-1} half width D, which we will refer to as the Doppler profile, and a Gaussian profile with the same width at half maximum as $\mathcal{N}(\delta)$ are also shown. When $\Delta = 0$ [Fig. 2(a)], Eq. (7)

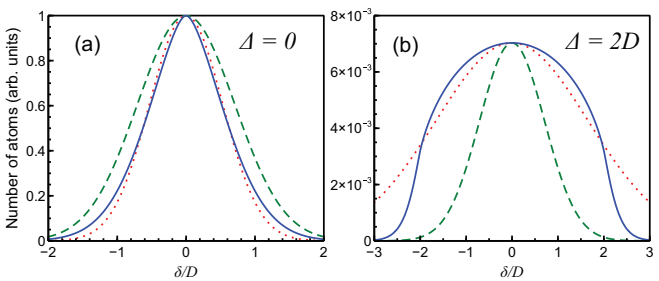

FIG. 2. (Color online) Double-resonant atom number function $\mathcal{N}(\delta)$ (solid) for two different pump detunings: (a) $\Delta = 0$ and (b) $\Delta = 2D$ (D is the e^{-1} Doppler half width). For comparison, a Gaussian of half width D (dashed) and a Gaussian with the same width at half maximum as $\mathcal{N}(\delta)$ (dotted) are shown.

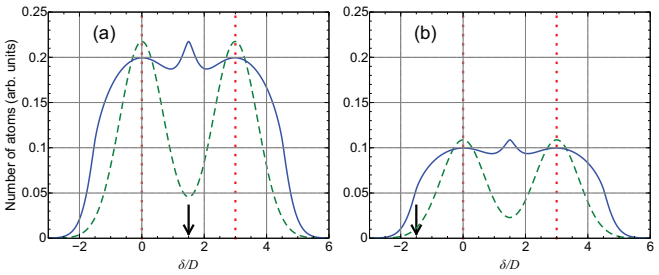

FIG. 3. (Color online) Number of double-resonant atoms with two transitions separated by $\omega_1 - \omega_0 = 3D$ (solid). The dotted lines correspond to the atomic transition frequencies. The arrow indicates the frequency of the pump field. (a) Symmetric pump field detuning $\Delta = 1.5D$. (b) Asymmetric pump field detuning $\Delta = -1.5D$. Dashed line: Sum of two Gaussian functions of e^{-1} half width D.

describes a sum of Gaussians centered at the origin, whose widths are narrower than D. As a result, $\mathcal{N}(\delta)$ is narrower at half maximum by a factor 0.753 than the Doppler profile. When $\Delta \neq 0$ [Fig. 2(b)] the peak value of the distribution is reduced by the factor $\exp[-(\Delta/D)^2]$. In this case, for small values of δ, $\mathcal{N}(\delta)$ is a slowly varying function until δ approaches $\pm\Delta$, where a steep decrease occurs.

The most striking difference between the distribution given by Eq. (7) and the distribution of double-resonant atoms when only two plane waves are considered is that the former is an even function of δ for any value of the pump detuning while the latter is generally not centered at $\delta = 0$ unless $\Delta = 0$ [see Eq. (4)]. The symmetry of $\mathcal{N}(\delta)$ around $\delta = 0$ is a consequence of the averaging over all possible relative orientations of the pump and probe fields.

The departure of $\mathcal{N}(\delta)$ from a Gaussian profile has significant spectral consequences. When the pump field is tuned to resonance with a given transition, the corresponding distribution of the double-resonant atoms is narrower than the Doppler profile. When the pump field is detuned from resonance, not only can the double-resonant atom profile be significantly broader than the Doppler profile, but also different spectral features arise. Such features are better appreciated when the atom possess two nearby transitions. Depending on the frequency of the pump field and the separation between the atomic transitions compared to the Doppler width, a large variety of line shapes can occur. Two examples are given in Fig. 3, where the number of double-resonant atoms is plotted for atoms with two transitions with a frequency separation $3D$. The narrow peak appearing around the line center is a consequence of the steepness of the decay of $\mathcal{N}(\delta)$ around $|\delta| \simeq |\Delta|$. Notice that the position of the pump field does not necessarily correspond to that of the central narrow peak.

B. Calculation of the excited-state population

With the D_1 hyperfine transitions of Rb in mind, we consider an atom with two ground levels g_1 and g_2 and two excited levels e_1 and e_2. Depending on the transitions addressed by each field, four possible kinds of level schemes can occur: a two-level system with two fields, a V system,

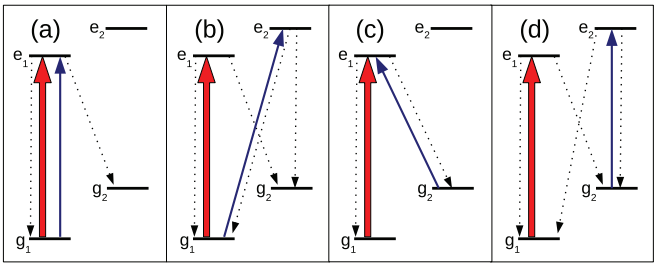

FIG. 4. (Color online) Field and level schemes for double-resonant atoms with two ground levels g_1,g_2 and two excited levels e_1,e_2. Solid arrows: Pump (thick) and probe (thin) fields. Dotted arrows: Spontaneous emission decay. Twelve similar additional schemes are obtained by interchanging the pump and probe fields or the atomic levels.

a Λ system, and two separate two-level systems. Examples of these level schemes are sketched in Fig. 4. A total of 16 level schemes arise on the D_1 line by interchanging the fields or the atomic levels. Each scheme corresponds to a different set of rate equations obtained by assuming isotropical and unpolarized light fields [22]. As an example, the rate equations for the case of the Λ system of Fig. 4(c) are

$$\dot{n}_{g_1} = -\left(\gamma + \frac{s_{1,1}I_1}{d_{g_1}}\right)n_{g_1} + \left(\Gamma p_{1,1} + \frac{s_{1,1}I_1}{d_{e_1}}\right)n_{e_1} + \gamma n_{10}, \tag{8a}$$

$$\dot{n}_{g_2} = -\left(\gamma + \frac{s_{2,1}I_2}{d_{g_2}}\right)n_{g_2} + \left(\Gamma p_{1,2} + \frac{s_{2,1}I_2}{d_{e_1}}\right)n_{e_1} + \gamma n_{20}, \tag{8b}$$

$$\dot{n}_{e_1} = \frac{s_{1,1}I_1}{d_{g_1}}n_{g_1} + \frac{s_{2,1}I_2}{d_{g_2}}n_{g_2} - \left[\gamma + \Gamma + \frac{(s_{1,1}I_1 + s_{2,1}I_2)}{d_{e_1}}\right]n_{e_1}, \tag{8c}$$

where n_{g_1}, n_{g_2}, and n_{e_1} are the level populations. Here Γ is the total excited-state decay rate, and γ is an overall decay rate affecting all states. In our system this rate accounts in a simplified way for the interruption of the light-atom interaction due to a collision with a pore wall. I_1 and I_2 are proportional to the intensities of the pump and probe fields, respectively, $s_{i,j}$ is a numerical coefficient representing the strength of the transition from g_i to e_j [23], $p_{i,j}$ is the probability for radiative decay from the excited level e_i to the ground level g_j, $d_{g_i(e_i)} \equiv 2F_i + 1$ is the degeneracy of level $g_i(e_i)$ (F_i is the total angular momentum), and n_{i0} are the ground level populations in the absence of light and for fresh atoms coming into the system. They are assumed to be thermal: $n_{i0} = n_0 d_{g_i}/(d_{g_1} + d_{g_2})$, where n_0 is the total number of atoms interacting with the two fields.

After obtaining the steady-state solution to the rate equation system we expand the total excited-state population $n_e = n_{e_1} + n_{e_2}$ into a power series of I_1 and I_2:

$$n_e = \eta_e^{(1)}I_1 + \eta_e'^{(1)}I_2 + \eta_e^{(2)}I_1I_2 + \cdots. \tag{9}$$

TABLE I. Transition strength coefficients $s_{i,j}$ for the D_1 transitions of the two Rb isotopes [22,23].

^{87}Rb	e_1 ($F=1$)	e_2 ($F=2$)	^{85}Rb	e_1 ($F=2$)	e_1 ($F=3$)
g_1 ($F=1$)	1/6	5/6	g_1 ($F=2$)	2/9	7/9
g_2 ($F=2$)	1/2	1/2	g_2 ($F=3$)	5/9	4/9

The expressions for $\eta_e^{(2)}$ corresponding respectively to the level schemes presented in Fig. 4 are given below:

$$\eta_e^{(2)} = -K2n_0\frac{s_{1,1}^2}{d_{g_1}}\left[p_{1,2} + x\left(1 + \frac{d_{g_1}}{d_{e_1}}\right)\right], \tag{10a}$$

$$\eta_e^{(2)} = -Kn_0\frac{s_{1,1}s_{1,2}}{d_{g_1}}(p_{1,2} + p_{2,2} + 2x), \tag{10b}$$

$$\eta_e^{(2)} = Kn_0s_{1,1}s_{2,1}\left[\frac{1}{d_{g_2}}\left(p_{1,2} - \frac{d_{g_2}}{d_{e_1}}x\right) + \frac{1}{d_{g_1}}\left(p_{1,1} - \frac{d_{g_1}}{d_{e_1}}x\right)\right], \tag{10c}$$

$$\eta_e^{(2)} = Kn_0s_{1,1}s_{2,2}\left(\frac{p_{1,2}}{d_{g_2}} + \frac{p_{2,1}}{d_{g_1}}\right), \tag{10d}$$

where $x = \gamma/\Gamma$ and $K = [\gamma\Gamma(dg_1 + dg_2)(1+x)^2]^{-1}$.

The terms on the right-hand side of Eqs. (10) that are proportional to the decay probabilities $p_{i,j}$ represent optical pumping while the terms proportional to x originate from saturation. The overall result of both processes corresponds to increased transparency in the case of Eqs. (10a) and (10b) and to increased absorption in the case of Eq. (10d) (notice the sign change). Equation (10c) is special since it corresponds to absorption for small x but reverses into transparency for $x > x_c$ with

$$x_c = \frac{d_{e_1}}{2}\left(\frac{p_{1,2}}{d_{g_2}} + \frac{p_{1,1}}{d_{g_1}}\right). \tag{11}$$

C. Calculation of the nonlinear signal

For a given value of the pump frequency, Eq. (7) is used to evaluate the total number of double-resonant atoms as a function of the probe frequency for all 16 possible transition pairs in a given isotope ($T = 393$ K is used). The obtained value is used as n_0 on each of Eqs. (10) for the determination of the excited-state population coefficient $\eta_e^{(2)}$ using the parameters given in Tables I and II [22,23]. The total nonlinear signal is given by the sum of all the $\eta_e^{(2)}$'s considering all level schemes in the D_1 transitions of ^{87}Rb and ^{85}Rb. In this calculation the only free parameter is x, which is the ratio

TABLE II. Spontaneous decay probabilities $p_{i,j}$ from excited level e_i to ground level g_j for the two Rb isotopes [23].

^{87}Rb	e_1 ($F=1$)	e_2 ($F=2$)	^{85}Rb	e_1 ($F=2$)	e_1 ($F=3$)
g_1 ($F=1$)	1/4	5/8	g_1 ($F=2$)	2/7	7/11
g_2 ($F=2$)	3/4	3/8	g_2 ($F=3$)	5/7	4/11

between the rate γ describing the loss (and renewal) of atoms interacting with light and the excited-state decay rate Γ.

IV. EXPERIMENTAL RESULTS AND DISCUSSION

Figure 5 shows the recorded nonlinear signal as a function of the probe-laser frequency for the two cells and for different values of the pump-laser frequency. Also shown in Fig. 5 are the corresponding calculated spectra. On each row the spectra are normalized to the same maximum. The only free parameter in the calculation $x = \gamma/\Gamma$ has been chosen to fit the observations of a given cell. Consistently we have used $x = 0.2$ for the large-grain cell and $x = 0.5$ for the small-grain cell. Notice that the choice of a single value of x for each cell results in a good agreement between experimental and calculated spectra for different values of the pump frequency.

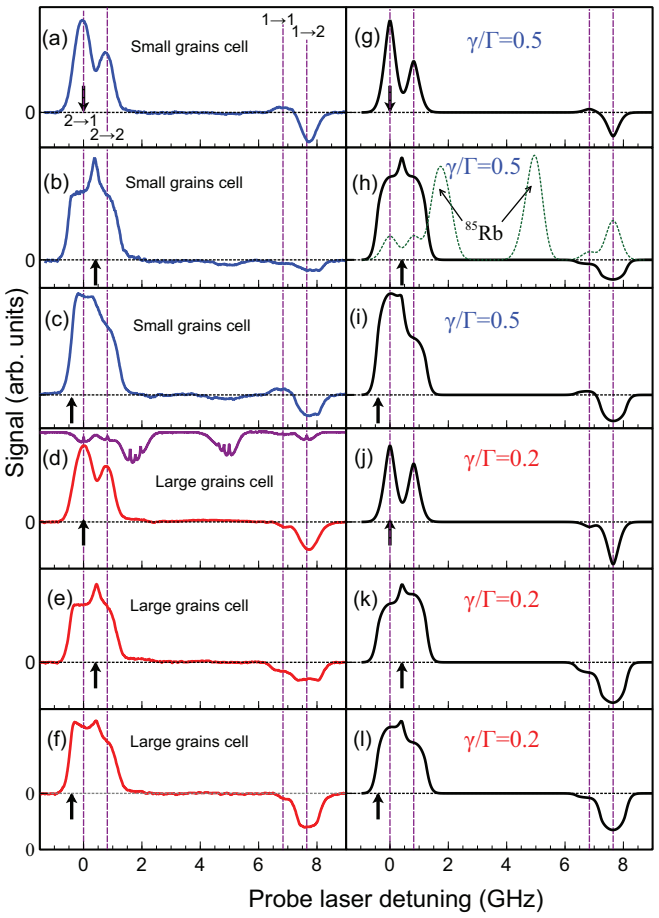

FIG. 5. (Color online) Nonlinear signal around the D_1 transitions of Rb as a function of probe frequency for different frequencies of the pump field. First column: Experimental signal. Second column: Corresponding calculated signal. The arrow indicates the pump-laser frequency. Two different cells were used (see text). Plots on the same row are normalized to the same maximum value. The value of $x = \gamma/\Gamma$ used in the calculation is given. The dotted curve in (h) is proportional to the calculated value of $\eta_e'^{(1)}$ giving the linear response to the probe field [see Eq. (9)]. The saturated absorption signal used for frequency calibration is shown in (d) (upper trace). Vertical dashed lines correspond to the frequencies of the hyperfine transitions $F_g \to F_e$ of ^{87}Rb.

The use of a larger value of x for the smaller-grain cell is consistent with the expectation of smaller pore dimensions and consequently with a larger decay rate γ due to the interruption of the atomic evolution by collisions with the pore walls. The figures for γ obtained from the values of x mentioned above are typical inverse time of flight for thermal atoms inside pores with tenth of microns dimensions. Interestingly enough, the value of x in the small-grain cell is larger than the value of $x_c = 0.35$ [see Eq. (11)] associated with the $F = 1 \to F' = 1$ transition. In consequence, the peak for this transition in the small-grain cell corresponds to gain instead of absorption [compare, for instance, Figs. 5(a) and 5(g) with Figs. 5(d) and 5(j)].

The nonlinear signal is highly isotope selective. Since the pump field is near the ^{87}Rb transitions, the contribution of ^{85}Rb atoms is very small.

Clearly visible in Fig. 5 is the departure of the nonlinear signal line shape from the usual Gaussian Doppler profile. For comparison Fig. 5(h) shows the calculated *linear* response to the probe field. Notice the resolved Gaussian shapes and the significant contribution of ^{85}Rb atom peaks. The spectra shown in Figs. 5(b) and 5(h), 5(e) and 5(k), 5(c) and 5(i), and 5(f) and 5(l) are clearly reminiscent of the line shapes presented in Fig. 3. They present the characteristic sharp peak halfway between the $F = 2$ to $F' = 1$ and $F = 2$ to $F' = 2$ transitions of ^{87}Rb, which is the consequence of the steepness of the flank of the double-resonant atom number distribution. The plots presented in Fig. 5 correspond to a pump field tuned around the $F_g = 2 \to F_e = 1$ transition of ^{87}Rb. We have checked that a similarly satisfactory agreement between observations and model is achieved when the pump is tuned to other frequencies within the Rb D_1 line.

In spite of the general agreement between the observations and the numerical modeling, some differences appear. In general, the spectral lines in the experimental plots are broader and the spectrum is less resolved than in the calculated spectra. Also, a visible, though small, contribution of ^{85}Rb atoms is present on several spectra of Fig. 5 [see, for instance, Figs. 5(b) and 5(e)]. We interpret these facts as owing to the frequency redistribution of light due to multiple absorption and reemission cycles. Indeed, we know from previous work that photon trapping is significant at the vapor density used in the experiments [20]. The frequency redistribution would result in an effective spectral broadening of the exciting light and consequently of the nonlinear signal line. Also, frequency redistribution can favor excitation of far-detuned ^{85}Rb transitions.

It is worth noticing that our crude modeling of a statistically complex physical process via simple rate equations results in good agreement with the experimental records. The theoretical modeling relies on a single parameter x. The calculated line shapes are very sensitive to the value of x that affects the relative weight and sign of the different peaks in the spectrum. As shown in Fig. 5, a proper choice of x allows a quite satisfactory reproduction of the overall line shape. Noticeable exceptions are the absorption dips at the $F_g = 1 \to F_e = 2$ transition in Figs. 5(b) and 5(e), which are overestimated in the calculation [Figs. 5(h) and 5(k)]. Whether this disagreement results from the above-mentioned frequency redistribution deserves further investigation.

V. CONCLUSION

We have presented the experimental study of incoherent pump-probe spectroscopy in Rb vapor confined to the micrometric interstices of porous glass. An essential characteristic of our system, the diffuse nature of light, introduces unusual and singular line shapes producing, under specific conditions, steep slopes and relatively narrow peaks in spite of the Doppler broadening due to the atomic motion. The origin of these narrow features was identified as a consequence of the averaging of the atomic response over all possible relative orientations of the pump and probe waves.

The disorder of the light as well as the variation in the atomic confinement geometry could in principle represent a major obstacle for the precise description of the light-atomic vapor interaction. However, we have shown that the assumption of complete randomness of these parameters allows a simplified and reliable theoretical treatment that correctly predicts a variety of spectra with only one free parameter related to the atom confinement. The relaxation of the assumption of complete light randomness is the motivation of future investigations. An extension of this work to temporal coherence spectroscopy with spatially random light is currently under way.

ACKNOWLEDGMENT

We wish to thank Athanasios Laliotis and Paulo Valente for motivating discussions.

[1] S. Briaudeau, D. Bloch, and M. Ducloy, Europhys. Lett. **35**, 337 (1996).
[2] S. Briaudeau, D. Bloch, and M. Ducloy, Phys. Rev. A **59**, 3723 (1999).
[3] G. Dutier, S. Saltiel, D. Bloch, and M. Ducloy, J. Opt. Soc. Am. B **20**, 793 (2003).
[4] G. Dutier, A. Yarovitski, S. Saltiel, A. Papoyan, D. Sarkisyan, D. Bloch, and M. Ducloy, Europhys. Lett. **63**, 35 (2003).
[5] J. Keaveney, A. Sargsyan, U. Krohn, I. G. Hughes, D. Sarkisyan, and C. S. Adams, Phys. Rev. Lett. **108**, 173601 (2012).
[6] J. Keaveney, I. G. Hughes, A. Sargsyan, D. Sarkisyan, and C. S. Adams, Phys. Rev. Lett. **109**, 233001 (2012).
[7] K. Fukuda, M. Kinoshita, A. Hasegawa, M. Tachikawa, and M. Hosokawa, J. Natl. Inst. Inf. Commun. Technol. Jpn. **50**, 95 (2003).
[8] H. Failache, A. Lezama, D. Bloch, and M. Ducloy, Europhys. Conf. Abstr. **28F**, 2 (2004).
[9] S. Knappe, L. Hollberg, and J. Kitching, Opt. Lett. **29**, 388 (2004).
[10] T. Varzhapetyan, D. Sarkisyan, L. Petrov, C. Andreeva, D. Slavov, S. Saltiel, A. Markovski, G. Todorov, and S. Cartaleva, Proc. SPIE **5830**, 196 (2005).
[11] A. Sargsyan, D. Sarkisyan, and A. Papoyan, Phys. Rev. A **73**, 033803 (2006).
[12] T. Svensson, M. Andersson, L. Rippe, J. Johansson, S. Folstad, and S. Andersson-Engels, Opt. Lett. **33**, 80 (2008).
[13] T. Svensson and Z. Shen, Appl. Phys. Lett. **96**, 021107 (2010).
[14] T. Svensson, E. Adolfsson, M. Lewander, C. A. Xu, and S. Svanberg, Phys. Rev. Lett. **107**, 143901 (2011).
[15] B. Redding, S. F. Lieu, R. Sarma, and H. Cao, Nat. Photon. **7**, 746 (2012).
[16] P. Ballin, E. Moufarej, I. Maurin, A. Laliotis, and D. Bloch, Appl. Phys. Lett. **102**, 231115 (2013).
[17] D. S. Wiersma, M. P. van Albada, and A. Lagendijk, Phys. Rev. Lett. **75**, 1739 (1995).
[18] Q. Baudouin, N. Mercadier, V. Guarrera, W. Guerin, and R. Kaiser, Nat. Phys. **9**, 357 (2013).
[19] M. Segev, Y. Silberberg, and D. N. Christodoulides, Nat. Photon. **7**, 197 (2013).
[20] S. Villalba, H. Failache, A. Laliotis, L. Lenci, S. Barreiro, and A. Lezama, Opt. Lett. **38**, 193 (2013).
[21] S. Villalba, A. Laliotis, L. Lenci, D. Bloch, A. Lezama, and H. Failache, Phys. Rev. A **89**, 023422 (2014).
[22] M. Auzinsh, D. Budker, and S. Rochester, *Optically Polarized Atoms: Understanding Light-Atom Interactions* (Oxford University Press, Oxford, UK, 2010).
[23] M. Weissbluth, *Atoms and Molecules* (Academic, London, 1978).